Electromagnetic Properties of Shielded Ring Lines and Attenuation of the Fundamental Dipolar Mode

CLAUDE FRAY AND ALBERT PAPIERNIK

Abstract—**This paper presents a theoretical analysis of the electromagnetic properties of the shielded ring line and provides expressions for field components, stored energy, and power flow. The dispersion relation obtained by equating electric and magnetic stored energies is discussed. The shielded ring line is shown to have a fundamental dipolar hybrid mode. The attenuation of this mode is evaluated. Measurements have corroborated the theoretical values.**

I. Introduction

THE OPEN RING LINE, operating in the fundamental dipolar hybrid mode, is a low-loss line [1]–[3] with significant extension of the fields around the line. Potential uses for the open line include railway traffic control and obstacle detection, and telecommunication applications when the line is shielded. In a previous study [4] of the shielded ring line in which the periodicity was neglected, the theoretical results did not agree well with experimental results when the period becomes greater than the ring radius. In this paper, we present more accurate results that take into account the periodicity. We assumed that the rings are infinitely thin, perfectly conducting tapes (Fig. 1) and postulate a current distribution on the rings. The field is expanded in eigenfunctions of the metallic cross section. A dispersion relation is obtained by equating magnetic and electric stored energies. Measurements have corroborated the calculated dispersion characteristics and attenuation of the fundamental dipolar hybrid mode.

II. Theoretical Formulation

A. Surface Current Density

To determine the surface current density, we assume that the rings are infinitely thin, perfectly conducting tapes with a width small compared with both the period and the wavelength (see Fig. 1). Under these conditions, it is permissible to neglect the longitudinal (z-directed) current. The field is produced only by the azimuthal current density as in the case of the open ring line [5]. With an $e^{j\omega t}$ factor omitted, we have

$$\boldsymbol{J}=\frac{I}{H}\cos n\theta\,\delta(r-a)\boldsymbol{u}_\theta\sum_{m=-\infty}^{\infty}D_m e^{-j\beta_m z}$$

$$\text{with}\begin{cases}\beta_m=\beta+2m\pi/H\\ D_m=J_0(m\pi w/H)\end{cases}\qquad(1)$$

where I is the total current on a ring, n is a positive integer which characterizes the dependance on θ, βH is the phase shift between adjacent rings, β_m is the phase constant of the mth harmonic, and D_m are the Fourier coefficients. The D_m depend on the choice of the current distribution across the ring width. As in the case of the open ring line, we shall postulate that the current distribution is the same as that of an isolated narrow thin ring [6].

B. Field Expansion into a Cylindrical Volume [7]

This expansion in eigenfunctions $\phi_{sq}(r,\theta)$, $\psi_{sq}(r,\theta)$ of the circles of radius b is

$$\boldsymbol{E}=\sum_s\sum_q\left\{a_{sq}\nabla\phi_{sq}+b_{sq}+b_{sq}(\boldsymbol{u}_z\times\nabla\psi_{sq})+c_{sq}\phi_{sq}\boldsymbol{u}_z\right\}$$

$$\boldsymbol{H}=\sum_s\sum_q\left\{\alpha_{sq}(\boldsymbol{u}_z\times\nabla\phi_{sq})+\beta_{sq}\nabla\psi_{sq}+\gamma_{sq}\psi_{sq}\boldsymbol{u}_z\right\}\qquad(2)$$

where the expressions of the eigenfunctions and of the corresponding eigenvalues μ_{sq} and ν_{sq} are

$$\phi_{sq}=\frac{(\xi/\pi)^{1/2}}{bJ_{s+1}(u_{sq})}J_s\left(u_{sq}\frac{r}{b}\right)\begin{Bmatrix}\sin s\theta\\ \cos s\theta\end{Bmatrix}$$

$$\mu_{sq}=\frac{u_{sq}}{b},\qquad u_{sq}\ q\text{th root of } J_s$$

$$\psi_{sq}=\frac{v_{sq}(\xi/\pi)^{1/2}}{b(v_{sq}^2-s^2)J_s(v_{sq})}J_s\left(v_{sq}\frac{r}{b}\right)\begin{Bmatrix}\sin s\theta\\ \cos s\theta\end{Bmatrix}$$

$$\nu_{sq}=\frac{v_{sq}}{b},\qquad v_{sq}\ q\text{th root of } J_s'\qquad(3)$$

with $s=0,1,2,3,\cdots,q=1,2,3,\cdots$, and $\xi=1$ for $s=0$ and $\xi=2$ for $s\neq 0$. These eigenfunctions are normalized

$$\int_S\phi_{sq}^2\,dS=\int_S\psi_{sq}^2\,dS=1.$$

The coefficients $a_{sq}(z)$, $b_{sq}(z)$, $c_{sq}(z)$, $\alpha_{sq}(z)$, $\beta_{sq}(z)$, and $\gamma_{sq}(z)$ are given by differential equations obtained from

Manuscript received July 24, 1978; revised December 1, 1978. This work was supported by the Centre National d'Etudes des Télécommunications.

The authors are with U.E.R. des Sciences, Laboratoire d'Electronique des Microondes, Equipe de Recherche Associée au CNRS, Université de Limoges, Limoges, France.

0018-9480/79/0400-0334$00.75

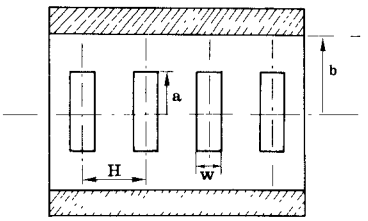

Fig. 1. Schematic representation of the shielded ring line (a ring radius, H period, w ring width, b shield radius).

expanding Maxwell's equations in eigenfunctions and considering the boundary conditions at $r=b$. These are

$$\frac{d^2a_{sq}}{dz^2}+\left(k^2-\mu_{sq}^2\right)a_{sq}=\frac{\mu_{sq}^2-k^2}{j\omega\epsilon\mu_{sq}^2}\int_S \boldsymbol{J}\cdot\nabla\phi_{sq}\,dS$$

$$\frac{d^2\alpha_{sq}}{dz^2}+\left(k^2-\mu_{sq}^2\right)\alpha_{sq}=-\frac{1}{\mu_{sq}^2}\frac{d}{dz}\int_S \boldsymbol{J}\cdot\nabla\phi_{sq}\,dS$$

$$c_{sq}=\frac{\mu_{sq}^2}{j\omega\epsilon}\alpha_{sq}\qquad \gamma_{sq}=\frac{\nu_{sq}^2}{j\omega\mu}b_{sq}$$

$$\frac{d^2b_{sq}}{dz^2}+\left(k^2-\nu_{sq}^2\right)b_{sq}=\frac{j\omega\mu}{\nu_{sq}^2}\int_S \boldsymbol{J}\cdot(\boldsymbol{u}_z\times\nabla\psi_{sq})\,dS$$

$$\frac{d^2\beta_{sq}}{dz^2}+\left(k^2-\nu_{sq}^2\right)\beta_{sq}=\frac{1}{\nu_{sq}^2}\frac{d}{dz}\int_S \boldsymbol{J}\cdot(\boldsymbol{u}_z\times\nabla\psi_{sq})\,dS \quad (4)$$

where $k=\omega(\epsilon\mu)^{1/2}=\omega/c$ denotes the wavenumber of the medium, ϵ the permittivity, μ the permeability, and c the light velocity. If we introduce the expressions (3) for the eigenfunctions into the differential equation (4), we easily obtain the coefficients, and then the field components are deduced from (2). These components are expressed as a double expansion: one in space harmonics and one in Fourier–Bessel or Dini series. The longitudinal components are given in Appendix A. After lengthy calculations, we found that the different series that appear in the component expressions can be summed (see Appendix B). After rearranging we obtain

where

$$\alpha_m^2=\beta_m^2-k^2$$

$$G_{nm}(a,r)=\{I_n(\alpha_m a)I_n(\alpha_m r)K_n(\alpha_m b)/I_n(\alpha_m b)\}-F_{nm}(a,r)$$

$$H_{nm}(a,r)=\{I_n(\alpha_m a)I_n(\alpha_m r)K_n'(\alpha_m b)/I_n'(\alpha_m b)\}-F_{nm}(a,r). \quad (6)$$

$F_{nm}(a,r)$ is a function already introduced for the open ring line study [5]

$$F_{nm}(a,r)=\begin{vmatrix} K_n(\alpha_m a)I_n(\alpha_m r), & r<a \\ I_n(\alpha_m a)K_n(\alpha_m r), & r>a \end{vmatrix} \quad (7)$$

and $Z=\sqrt{\mu/\epsilon}$ is the impedance of the medium.

C. Component Analysis

The modes of the shielded ring line are of the hybrid type, except for the special case of circular symmetry ($n=0$) and cutoff ($\beta=0$). Indeed, for $n=0$, or $\beta=0$, the components in (5) are reduced to three components E_θ, H_z, H_r, or E_r, E_θ, H_z, respectively, which correspond to the TE_{0q} modes over the passband or to the TE_{nq} modes at cutoff. The TM_{0q} modes over the passband and the TM_{nq} modes at cutoff can also propagate in the shielded ring line but do not appear in the field component expressions in (5) because there is no coupling to the ring current (i.e., $E_\theta=H_z=0$ on the rings). When the shield radius b tends to infinity, the functions $G_{nm}(a,r)$ and $H_{nm}(a,r)$ (6) tend to the function $F_{nm}(a,r)$ (7), and the components (5) tend to those of the open ring line [5].

$$E_z=-\frac{ZI}{kH}n\sin n\theta\sum_{m=-\infty}^{\infty}D_m\beta_m G_{nm}(a,r)e^{-j\beta_m z}$$

$$E_r=-j\frac{ZI}{kH}n\sin n\theta\sum_{m=-\infty}^{\infty}\frac{D_m}{\alpha_m^2}\left\{\beta_m^2\frac{\partial G_{nm}(a,r)}{\partial r}+k^2\frac{a}{r}\frac{\partial H_{nm}(a,r)}{\partial a}\right\}e^{-j\beta_m z}$$

$$E_\theta=-j\frac{ZI}{kH}\cos n\theta\sum_{m=-\infty}^{\infty}\frac{D_m}{\alpha_m^2}\left\{\frac{n^2}{r}\beta_m^2 G_{n,m}(a,r)+k^2 a\frac{\partial^2 H_{nm}(a,r)}{\partial a\partial r}\right\}e^{-j\beta_m z}$$

$$H_z=a\frac{I}{H}\cos n\theta\sum_{m=-\infty}^{\infty}D_m\frac{\partial H_{nm}(a,r)}{\partial a}e^{-j\beta_m z}$$

$$H_r=j\frac{I}{H}\cos n\theta\sum_{m=-\infty}^{\infty}D_m\frac{\beta_m}{\alpha_m^2}\left\{\frac{n^2}{r}G_{nm}(a,r)+a\frac{\partial^2 H_{nm}(a,r)}{\partial r\partial a}\right\}e^{-j\beta_m z}$$

$$H_\theta=-j\frac{I}{H}n\sin n\theta\sum_{m=\infty}^{\infty}D_m\frac{\beta_m}{\alpha_m^2}\left\{\frac{\partial G_{nm}(a,r)}{\partial r}+\frac{a}{r}\frac{\partial H_{nm}(a,r)}{\partial a}\right\}e^{-j\beta_m z} \quad (5)$$

III. Energy and Dispersion Relations

A. Stored Energy Per Unit Length and Power Flow

The expressions for these quantities can be determined from the components after summation of the Fourier–Bessel and Dini series (5) or before summation (Appendix A). We have selected the second method because it allows the use of orthogonality properties of the eigenfunctions. After rearranging, the final expressions of stored magnetic energy $\overline{W}_M$, stored electric energy $\overline{W}_E$, and power flow P can be written

$$\frac{c\overline{W}_M}{ZI^2}=\frac{\pi}{4H^2}\sum_{m=-\infty}^{\infty}\frac{D_m^2}{\alpha_m^2}\left\{n^2\beta_m^2G_{nm}(a,r)+\beta_m^2a^2\frac{\partial^2H_{nm}(a,r)}{\partial a\partial r}+n^2\beta_m^2\left\{\frac{I_n^2(\alpha_ma)}{2I_n^2(\alpha_mb)}-a\frac{\partial G_{nm}(a,a)}{\partial a}\right\}-\alpha_m^2k^2a^2\left\{\left(1+\frac{n^2}{\alpha_m^2a^2}\right)\frac{I_n'^2(\alpha_ma)}{2I_n'^2(\alpha_mb)}+a\left(1+\frac{n^2}{\alpha_m^2b^2}\right)\frac{\partial H_{nm}(a,a)}{\partial a}\right\}\right\}$$

$$\frac{c\overline{W}_E}{ZI^2}=\frac{\pi}{4H^2}\sum_{m=-\infty}^{\infty}\frac{D_m^2}{\alpha_m^2}\left\{n^2\frac{\beta_m^2}{k^2}(k^2-\alpha_m^2)G_{nm}(a,a)+k^2a^2\frac{\partial^2H_{nm}(a,a)}{\partial a\partial r}+n^2\beta_m^2\left\{\frac{I_n^2(\alpha_ma)}{2I_n^2(\alpha_mb)}-a\frac{\partial G_{nm}(a,a)}{\partial a}\right\}-\alpha_m^2k^2a^2\left\{\left(1+\frac{n^2}{\alpha_m^2a^2}\right)\frac{I_n'^2(\alpha_ma)}{2I_n'^2(\alpha_mb)}+a\left(1+\frac{n^2}{\alpha_m^2b^2}\right)\frac{\partial H_{n,m}(a,a)}{\partial a}\right\}\right\} \tag{8}$$

$$\frac{P}{ZI^2}=\frac{\pi}{2kH^2}\sum_{m=-\infty}^{\infty}D_m^2\frac{\beta_m^2}{\alpha_m^4}\left\{n^2k^2G_{nm}(a,a)+k^2a^2\frac{\partial^2H_{nm}(a,a)}{\partial a\partial r}+n^2\beta_m^2\left\{\frac{I_n^2(\alpha_ma)}{2I_n^2(\alpha_mb)}-a\frac{\partial G_{nm}(a,a)}{\partial a}\right\}-k^2a^2\alpha_m^2\left\{\left(1+\frac{n^2}{\alpha_m^2a^2}\right)\frac{I_n'^2(\alpha_ma)}{2I_n'^2(\alpha_mb)}+a\left(1+\frac{n^2}{\alpha_m^2b^2}\right)\frac{\partial H_{nm}(a,a)}{\partial a}\right\}\right\}. \tag{9}$$

B. Dispersion Relation and Group Velocity

The dispersion relation is obtained by specifying that $\overline{W}_M=\overline{W}_E$ [8]

$$\sum_{m=-\infty}^{\infty}D_m^2\left\{n^2\frac{\beta_m^2}{\alpha_m^2}I_n^2(\alpha_ma)\left\{\frac{K_n(\alpha_mb)}{I_n(\alpha_mb)}-\frac{K_n(\alpha_ma)}{I_n(\alpha_ma)}\right\}+k^2a^2I_n'^2(\alpha_ma)\left\{\frac{K_n'(\alpha_mb)}{I_n'(\alpha_mb)}-\frac{K_n'(\alpha_ma)}{I_n'(\alpha_ma)}\right\}\right\}=0. \tag{10}$$

The group velocity in a periodic structure is equal to the energy velocity [8] and is given by

$$v_g=\frac{d\beta}{d\omega}=\frac{P}{\overline{W}_E+\overline{W}_M}=\frac{P}{\overline{W}}. \tag{11}$$

IV. Modes of the Shielded Ring Line

The solution of the dispersion relation (10) gives the dispersion curves. In order to reduce the computation time, we have chosen to integrate (11), which can be written as

$$\frac{dy}{dx}=F(x,y) \text{ where } x=\beta H,\ y=kH \text{ and } F(x,y)=P/c\overline{W}.$$

This first-order differential equation is solved numerically using a fourth-order Runge–Kutta integration process with initial condition $y(x_0)=y_0$ obtained by solving the dispersion relation for $x_0=0$. The method provides us with the dispersion curves, stored energy, power flow, and group velocity. Dispersion curves of a particular shielded ring line are illustrated in Fig. 2. Limit values, obtained from the fundamental term of the dispersion relation (10), are represented in the figure by double arrows. These values correspond to the nonperiodic theory [4] in which the ring line is assumed to be an ideal cylinder with conduction in the ring direction only (space harmonics neglected). Two types of modes appear: the circular symmetry and the hybrid modes.

The circularly symmetric modes comprise: 1) the TE_{0q} modes, analogous to those of smooth guides of diameter $2a$ and those of the coaxial guide (a,b) ($TE_{0q}(a,b)$ on the figure) perturbed by the rings; 2) the TM_{0q} modes (TM_{01}, TM_{02} on the figure) of the smooth guide of diameter $2b$ unperturbed by the rings.

The EH_{nq} hybrid modes (qth mode of n-fold symmetry in θ encountered in a scale of increasing frequencies) may be divided into two groups: 1) the EH_{n1} modes (EH_{11}, EH_{21}, EH_{31}, EH_{41} on the figure), the cutoff of which is TE_{n1} coaxial for any geometrical parameters, can be termed "fast" ($\omega/\beta>c$) or "slow" ($\omega/\beta<c$) according to the frequency; 2) the $EH_{nq}(q>1)$ modes (EH_{12}, EH_{13}, EH_{22}, EH_{23} on the figure), the cutoff of which is TE or TM according to the values of the geometrical parameters, are always "fast." The interchange of cutoff frequencies of two adjacents $EH_{nq}(q>1)$ modes are explained by the coupling between modes of the same θ symmetry according to Pierce and Tien theory [9]. When the dispersion curves of two modes EH_{nq} and $EH_{nq+1}(q>1)$ are almost coincident, the characteristic of the EH_{nq} mode is distorted having a minimum beyond cutoff in the fast-wave domain (for example the EH_{22} mode on the figure).

An experimental verification of the dispersion curves has been made which corroborates the theoretical results

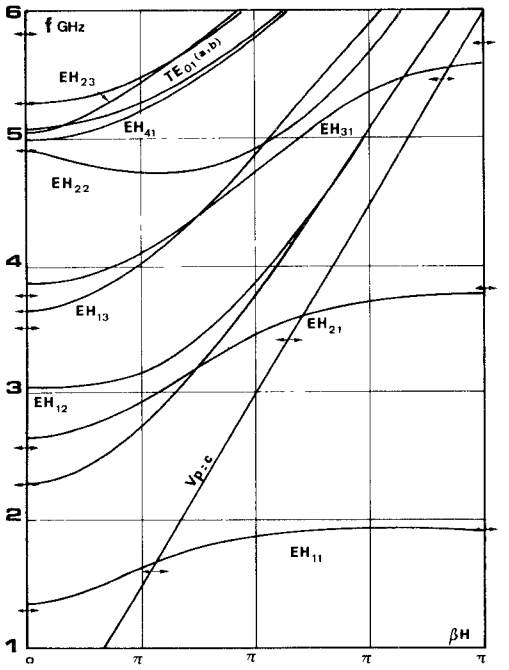

Fig. 2. Theoretical dispersion curves for the first modes ($H=2.5$ cm, $2a=5$ cm, $2b=10$ cm, $w=0.5$ cm). The double arrows are obtained by neglecting the guide periodicity.

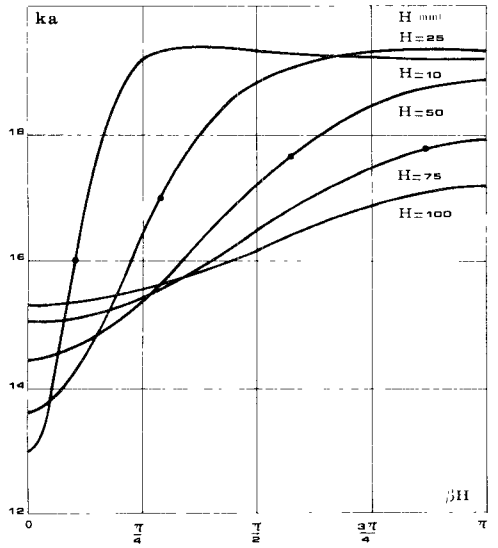

Fig. 3. Dispersion curve of the EH_{11} mode as the period H increases from 1 to 10 cm with $2b=10$ cm, $2a=5$ cm, $w=0.5$ cm.—·—point where the dispersion curve cuts the straight $v_p=c$.

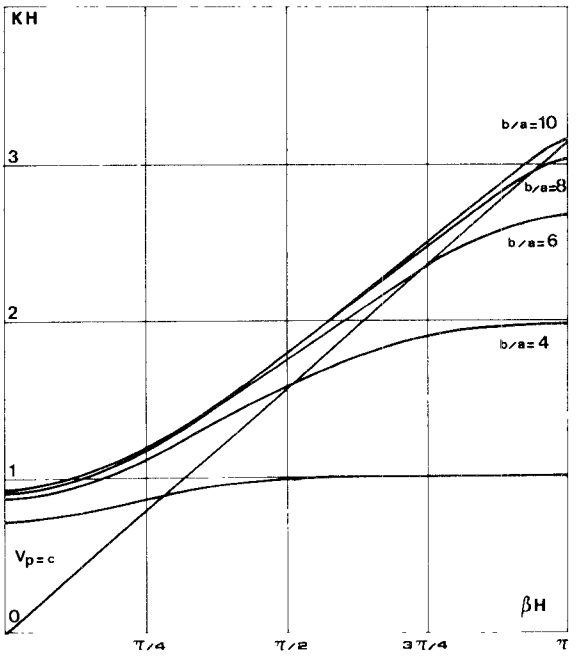

Fig. 4. Dispersion curve of the EH_{11} mode as the ring radius a decreases with $H=2.5$ cm, $2b=10$ cm, $w=0.5$ cm.

{10}. To measure the dispersion curves of the first few modes, a resonant cavity was formed by placing shorting end plates at symmetry planes halfway between the rings. Two teflon supports were holding up the rings. The discrepancy between theoretical and experimental dispersion curves is less than 1 and 1.5 percent for the EH_{11} and EH_{21} modes, respectively. It can be explained almost entirely by the spurious effect of the dielectric supports which tend to lower the resonant frequencies.

Fig. 3 exhibits the very significant role of the guide period on the dispersion curve. This result shows that the new theory presented here, which takes into account the guide periodicity, is needded for accuracy. The values of the period H, the ring radius a, and the shield radius b influence considerably the dispersion curves of the EH_{n1} modes, but the ring width w has little influence: the passband decreases when the period increases (Fig. 3) while it extends toward the high frequencies as the ring radius decreases (Fig. 4) and toward the low frequencies

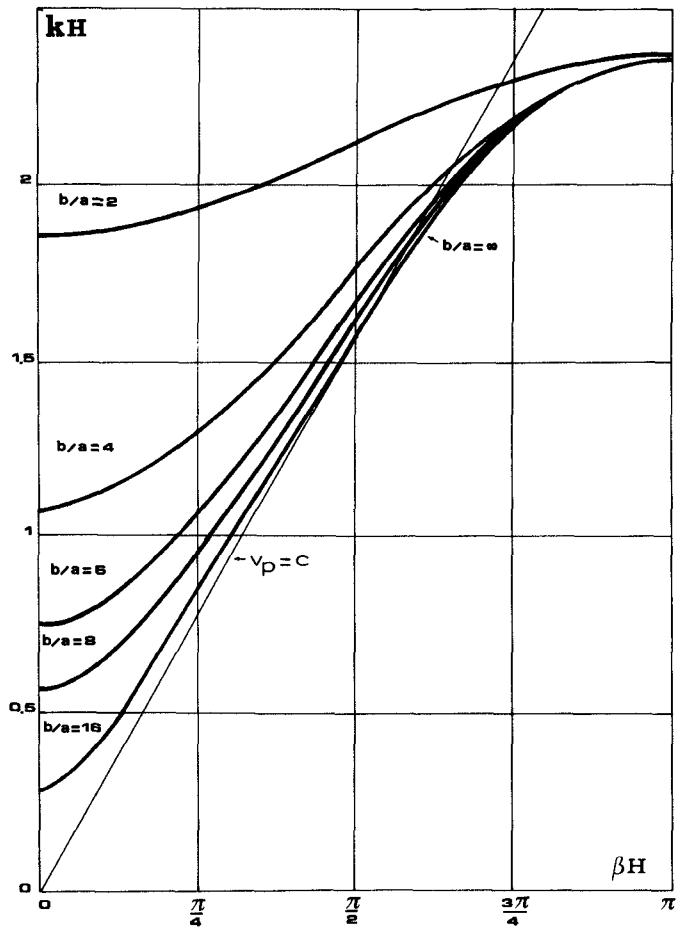

Fig. 5. Dispersion curve of the EH_{11} mode as the shield radius increases with $H=2.5$ cm, $2a=2$ cm, $w=0.5$ cm.

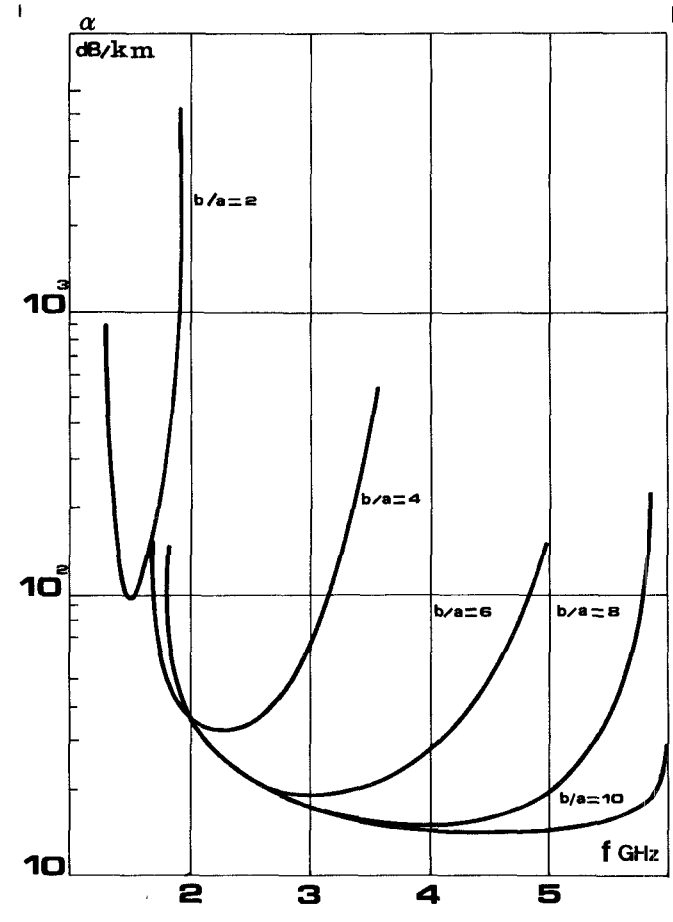

Fig. 6. Attenuation variation as the ring radius a decreases with $H=2.5$ cm, $2b=10$ cm, $w=0.5$ cm.

as the shield radius increases (Fig. 5). When b tends to infinity, the shielded ring line tends to coincide with the open ring line, and the EH_{n1} modes become the same as those of the open ring line. The fundamental mode of the shielded ring line is, therefore, a dipolar hybrid mode, as is the case for the unshielded line.

V. Attenuation of the Fundamental Dipolar Mode EH_{11}

The following relation gives the longitudinal attenuation constant where P, P_r, P_s are, respectively, the power flow (9), the ohmic losses per unit axial length on the rings and on the shield:

$$\alpha = \frac{P_r + P_s}{2P} 8.68\ 10^3 \text{ dB/km} \qquad (12)$$

with

$$P_r = \frac{\pi I^2}{2} R_S \frac{a}{Hw} \qquad R_S = \sqrt{\omega\mu/2\sigma}$$

(μ: permeability and σ: conductivity)

$$P_s = \frac{\pi I^2}{H^2} R_S \frac{a^2}{b^2} \sum_{m=-\infty}^{\infty} D_m^2 \left\{ \frac{I_n'^2(\alpha_m a)}{I_n'^2(\alpha_m b)} + n^2 \frac{\beta_m^2}{\alpha_m^2} \left(\frac{I_n(\alpha_m a)}{\alpha_m a I_n(\alpha_m b)} - \frac{I_n'(\alpha_m a)}{\alpha_m b I_n'(\alpha_m b)} \right)^2 \right\}.$$

This simple expression for P_r represents an estimate of the ohmic losses. It is based on the assumption that the current distribution is a constant on both sides of the ring surfaces. The attenuation of the EH_{11} mode has been investigated with the help of the relation (12), and is determined chiefly by the ratio b/a. The period and ring width have a negligible influence when w/H is small. When b/a increases, either with b a constant or with a a constant, the attenuation becomes smaller and smaller over a broader and broader frequency band toward high frequencies (Fig. 6) with b kept a constant or toward low frequencies (Fig. 7) with a kept a constant. Thus the greater the distance from the rings to the shield, the smaller the attenuation of the EH_{11} mode.

Waveguide attenuations are measured by the cavity method. The attenuation coefficient is related to the Q factor Q_0 due to the shield and ring losses through the formula: $\alpha = \omega/2v_g Q_0$ where v_g denotes the group velocity of mode causing resonance. Q_0 is deduced from the measured Q factor of the cavity by eliminating losses on the end plates of the cavity. It is measured for several values of cavity length at the same frequency by the transmission method with negligible coupling.

Fig. 8 shows the theoretical and experimental attenuation of the dipolar mode for an aluminium alloy structure

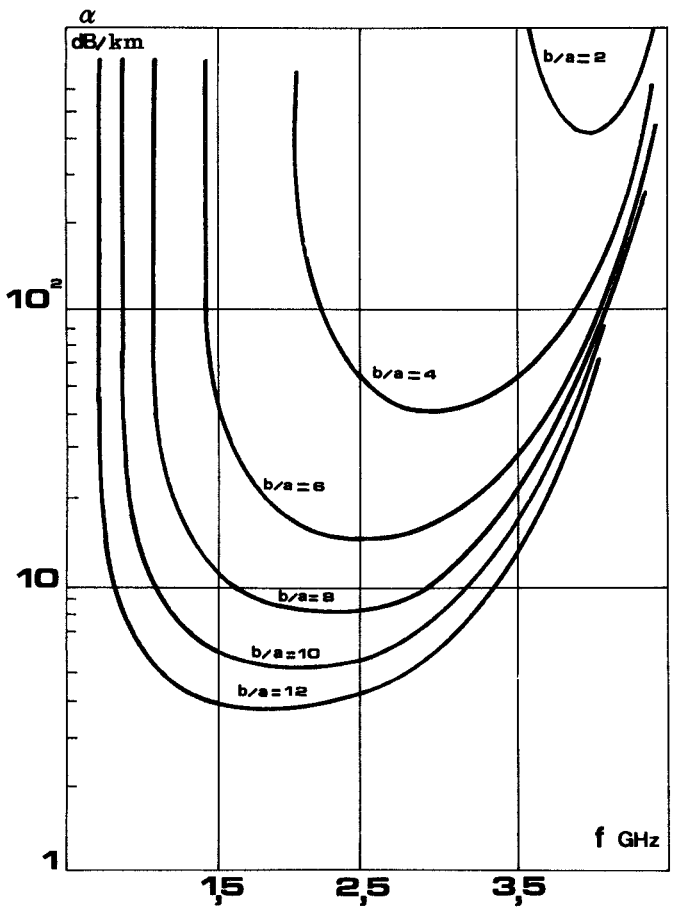

Fig. 7. Attenuation variation as the shield radius b increases with $H=2.5$ cm, $2a=2$ cm, $w=0.5$ cm.

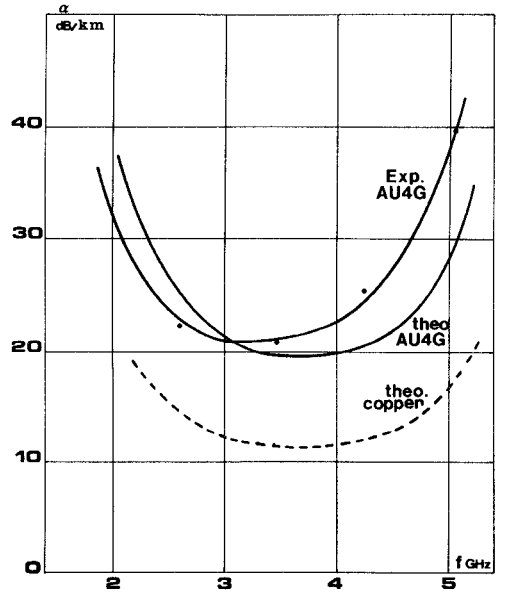

Fig. 8. Experimental and theoretical attenuation for the EH_{11} mode with $H=2.5$ cm, $2b=10$ cm, $2a=1.3$ cm ($b/a=0.7$), $w=0.5$ cm, and ring thickness is 0.05 cm.

(AU4G) with $b/a=7.7$. The rings are supported by a 2-mm-thick teflon pipe. The experimental curve is slightly shifted compared to the theoretical curve. This discrepancy may be explained by the effect of the teflon pipe that holds the rings and the experimental errors in the determination of the Q factor. The measured attenuation is less than 20 dB/km over a bandwidth of 1 GHz, and would be reduced to about 12 dB/km if the aluminium alloy were replaced by copper (Fig. 8).

VI. Conclusions

Our theoretical analysis of the shielded ring line was based on a postulated current distribution on the rings. It provides detailed knowledge of the properties of that guiding structure and analytical expressions for the field and energy relations. We found modes analogous to those of the disk-loaded waveguide or of the shielded dielectric line and, in addition, modes similar to those of the coaxial guide. The latter are circularly symmetric TE_{0q} modes and hybrid modes with cutoff close to that of TE_{nq} coaxial modes. EH_{n1} modes are the only ones that can propagate as slow waves. The fundamental mode of this periodic structure is the EH_{11} mode, whereas that of the disk-loaded waveguide is the TM_{01} mode. These EH_{n1} modes give those of the open ring line when the shield radius tends to infinity. If the open ring line operates in this dipolar hybrid mode as a low-loss line (the attenuation measured with an aluminum alloy structure being less than 5 dB/km [1], this property disappears partly when the line is shielded (about 12 dB/km for a copper structure).

Appendix A

$$E_z = \frac{ZI}{kH} n \sin n\theta \sum_{m=-\infty}^{\infty} 2 \cdot \sum_{q=1}^{\infty} \frac{D_m \beta_m J_n(u_{nq} a/b)}{(u_{nq}^2 + \alpha_m^2 b^2) J_{n+1}^2(u_{nq})} J_n\left(u_{nq} \frac{r}{b}\right) e^{-j\beta_m z}$$

$$H_z = -\frac{I}{H} a \cos n\theta \sum_{m=-\infty}^{\infty} 2 \cdot \sum_{q=1}^{\infty} \frac{D_m v_{nq}^3 J_n'(v_{nq}(a/b))}{b(v_{nq}^2 - n^2)(v_{nq}^2 + \alpha_m^2 b^2) J_n^2(v_{nq})} J_n\left(v_{nq} \frac{r}{b}\right) e^{-j\beta_m z}.$$

The definition of the Fourier–Bessel and Dini series is given in [11] and [12]: Fourier–Bessel series

$$f_n(y) = \sum_{q=1}^{\infty} L_{nq} J_n(u_{nq} y)$$

and Dini series

$$d_n(y) = \sum_{q=1}^{\infty} M_{nq} J_n(v_{nq} y)$$

with

$$L_{nq} = \frac{2}{J_{n+1}^2(u_{nq})} \int_0^1 t f_n(t) J_n(u_{nq} t)\, dt$$

$$M_{nq} = \frac{2v_{nq}^2}{(v_{nq}^2 - n^2) J_n^2(v_{nq})} \int_0^1 t d_n(t) J_n(v_{nq} t)\, dt.$$

APPENDIX B

$$2\sum_{q=1}^{\infty}\frac{J_n(u_{nq}a)J_n(u_{nq}y)}{u_{nq}^2(u_{nq}^2+\mu^2)J_{n+1}^2(u_{nq})}=\frac{1}{\mu^2}\begin{vmatrix} y^n/2n\{a^{-n}-a^n\}+I_n(\mu y)\{I_n(\mu a)K_n(\mu)/I_n(\mu)-K_n(\mu a)\}, & 0\leqslant y\leqslant a\leqslant 1\\ a^n/2n\{y^{-n}-y^n\}+I_n(\mu a)\{I_n(\mu y)K_n(\mu)/I_n(\mu)-K_n(\mu y)\}, & 0\leqslant a\leqslant y\leqslant 1\end{vmatrix}$$

$$2\sum_{q=1}^{\infty}\frac{J_n^2(u_{nq}a)}{(u_{nq}^2+\mu^2)^2J_{n+1}^2(u_{nq})}=-\frac{I_n^2(\mu a)}{2\mu^2I_n^2(\mu)}+\frac{a}{\mu}\left\{I_n'(\mu a)I_n(\mu a)\frac{K_n(\mu)}{I_n(\mu)}-\frac{1}{2}\{K_n(\mu a)I_n'(\mu a)+I_n(\mu a)K_n'(\mu a)\}\right\}$$

$$2\sum_{q=1}^{\infty}\frac{v_{nq}^2}{v_{nq}^2-n^2}\frac{J_n(v_{nq}a)J_n(v_{nq}x)}{v_{nq}^2(v_{nq}^2+\mu^2)J_n^2(v_{nq})}=\frac{1}{\mu^2}\begin{vmatrix} \frac{x^n}{2n}\{a^n+a^{-n}\}+I_n(\mu x)\left\{I_n(\mu a)\frac{K_n'(\mu)}{I_n'(\mu)}-K_n(\mu a)\right\}, & 0\leqslant x\leqslant a\leqslant 1\\ \frac{a^n}{2n}\{x^n+x^{-n}\}+\left\{I_n(\mu x)\frac{K_n'(\mu)}{I_n'(\mu)}-K_n(\mu x)\right\}I_n(\mu a), & 0\leqslant a\leqslant x\leqslant 1\end{vmatrix}$$

$$2\sum_{q=1}^{\infty}\frac{v_{nq}^4}{v_{nq}^2-n^2}\frac{J_n'^2(v_{nq}a)}{(v_{nq}^2+\mu^2)^2J_n^2(v_{nq})}=\left(1+\frac{n^2}{\mu^2}\right)\frac{I_n'^2(\mu a)}{2I_n'^2(\mu)}+\mu a\left(1+\frac{n^2}{\mu^2a^2}\right)\cdot\left\{I_n(\mu a)I_n'(\mu a)\frac{K_n'(\mu)}{I_n'(\mu)}-\frac{1}{2}\{I_n(\mu a)K_n'(\mu a)+I_n'(\mu a)K_n(\mu a)\}\right\}.$$

REFERENCES

[1] A. Papiernik and C. Fray, "Low-loss open transmission line: The open ring line," *Electron. Lett.*, vol. 11. no. 10, pp. 209–210, 1975.

[2] C. Fray and A. Papiernik, "Theoretical and experimental attenuation of the open ring line," presented at the 6th European Microwave Conf., Rome, Italy, Sept. 14–16, 1976.

[3] ——, "The open ring line: A low loss surface waveguide," *IEEE Trans. Microwave Theory Tech.*, vol. MTT-26, pp. 886–894, Nov. 1978.

[4] Y. Garault and C. Fray, "Electromagnetic wave propagation in the shielded ring line," *IEEE Trans. Microwave Theory Tech.*, vol. MTT-22, pp. 92–99, Feb. 1974.

[5] C. Fray and A. Papiernik, "Theoretical analysis of open ring line," presented at the 1976 Int. Microwave Symp., Cherry Hill, NJ, June 14–16, 1976.

[6] S. Sensiper, "Electromagnetic wave on helical conductors," M.I.T. Res. Lab. Electr., Cambridge, MA, Rep. 194, May 1951.

[7] J. Van Bladel, *Electromagnetic Field*. New York: McGraw-Hill, 1964, pp. 417–422.

[8] D. A. Watkins, *Topics in Electromagnetic Theory*. New York: Wiley, 1958.

[9] J. R. Pierce and P. K. Tien, "Coupling of modes in helixes," *Proc. IRE*, vol. 42, pp. 1389–1396, Aug. 1954.

[10] C. Fray, "Propriétés électromagnétiques de la ligne à anneaux ouverte ou fermée," thesis, Univ. of Limoges, Limoges, France, May 1977.

[11] C. N. Watson, *A Treatise on the Theory of Bessel Functions*. New York: Cambridge, 1966, chap. VIII, pp. 516–617.

[12] G. Petiau, *La Théorie des Fonctions de Bessel*, Ed. CNRS, 1965.

A General Reciprocity Theorem

PAUL R. McISAAC, MEMBER, IEEE

***Abstract*—A general reciprocity theorem based on the Onsager relations is developed which applies to all causal and linear media, including those whose ac susceptibilities depend on an applied dc magnetic field and on the dc drift velocity of charge carriers. Applications are made to the scattering matrix for microwave junctions and to the mode orthogonality relations for uniform and periodic waveguides.**

Manuscript received June 23, 1978; revised October 23, 1978. This work was supported in part by the Air Force Office of Scientific Research under Contract F49620-77-C-0069.

The author is with the School of Electrical Engineering, Cornell University, Ithaca, NY 14853.

I. INTRODUCTION

ONE OF THE BASIC theorems of electromagnetic theory is the reciprocity theorem. There has been a long history of contributions to its development [1]–[6]. It is the purpose of this contribution to extend the range of applicability of the reciprocity theorem and to provide a physical basis for it through the Onsager relations. The requirements are only that the media in the region under consideration be causal and linear; they may be either passive or active. In particular, media whose ac suscept-

0018-9480/79/0400-0340$00.75